Check for updates

Characterizing Radiation Effectiveness in Ion-Beam Therapy Part II: Microdosimetric Detectors

Paolo Colautti[1], Giulio Magrin[2]*, Hugo Palmans[2,3], Miguel A. Cortés-Giraldo[4] and Valeria Conte[1]

[1] Istituto Nazionale di Fisica Nucleare (INFN), Laboratori Nazionali di Legnaro, Legnaro, Italy, [2] MedAustron Ion Therapy Center, Wiener Neustadt, Austria, [3] National Physical Laboratory, Teddington, United Kingdom, [4] Department of Atomic, Molecular and Nuclear Physics, Universidad de Sevilla, Sevilla, Spain

The specific advantages of ion beams for application in tumor therapy are attributed to their different macroscopic and microscopic energy deposition pattern as compared to conventional photon radiation. On the macroscopic scale, the dose profile with a Bragg peak at the highest depths and small lateral scattering allow a better conformation of the dose to the tumor. On the microscopic scale, the localized energy deposition around the trajectory of the particles leads to an enhanced biological effectiveness, typically expressed in terms of clinically significant relative biological effectiveness (RBE). Experimental investigations reveal complex dependencies of RBE on many physical and biological parameters, as e.g. ion species, dose, position in the field, and cell or tissue type. In order to complement the experimental work, different approaches are used for the characterization of the specific physical and biological properties of ion beams. In a set of two papers, which are linked by activities within a European HORIZON 2020 project about nuclear science and application (ENSAR2), we describe recent developments in two fields playing a key role in characterizing the increased biological effectiveness. These comprise the biophysical modeling of RBE and the microdosimetric measurements in complex radiation fields. This second paper focuses on microdosimeters and on the importance of providing the instrumental measurement of the spectra of the imparted energy. The relevance of microdosimetric quantities, complementary to the absorbed dose is emphasized. This parts provides an overview of the microdosimetric concepts and the recent experimental developments in the field of microdosimetry applied to ion beam therapy. Finally, a non-exhaustive, dedicated section in included to emphasize the relevance of Monte Carlo simulations as tool for the design of the microdosimetric detectors and for the interpretation of the experimental results. For the two distinctive clinical beams of protons and carbon ions, the lineal-energy parameters are correlated to the clinical concept of Linear Energy Transfer (LET) and RBE. The possibilities of applying experimental microdosimetry in ion-beam therapy are discussed considering the consolidated irradiation characteristics as well as the most recent developments.

Keywords: microdosimetry, ion-beam therapy, hadrontherapy, protontherapy, linear energy transfer (LET), relative biological effectiveness (RBE), monte–carlo simulation

INTRODUCTION

This work is the second of two parts focusing on characterizing radiation effectiveness in ion-beam therapy. The first part, on biophysical modeling of relative biological effectiveness (RBE), is published by Scholz et al. [1]. It is cited in this work as "Part I." Part I includes a general introduction on the concepts and the rationale of ion-beam therapy as well as the essential equations that describe the biophysical and physical quantities for the characterization of radiation effectiveness.

When high-energy photons are used in the clinic to treat tumors, there is a unique relationship between the absorbed dose, which is proportional to the photon fluence, and the relative number of surviving cells. When light ions are used, this unique relationship does not hold anymore: the number of surviving cells at distinct points in the patient's body can be different even if the absorbed dose in those points is the same. Equal physical doses of different radiation types do not always result in the same amount of biological damage. This fact suggests that the radiation capability of damaging living cells depends not only on the mean value of energy imparted but also on the microscopic probability distribution of energy imparted at the subcellular level. When deciding on a dose prescription for a new ion beam, the radiation oncologist has to take into account the varying effectiveness of radiation within various regions (depths) in the irradiated tissue [2]. A scaling factor known as the *RBE* is used to evaluate the biological effective dose. The *RBE* is defined as the ratio of a dose of photons to a dose of any other particle to obtain the same radiobiological effect. The *RBE* varies, among other factors, with the radiation quality (type and velocity of the ion), with the biological end point, with dose, and with dose rate [3]. However, it has been found that *RBE* depends, to a first approximation, on the linear energy transfer (*LET*), the average amount of energy that an ionizing particle transfers by purely "electronic" interactions (ionization or excitation) to the material traversed per unit distance. It is worth noticing that *LET* is a non-stochastic quantity, being an average, and it is strictly defined at a point of energy transfer. However, irradiation targets always have a finite volume, rather than being a dimensionless point, and the interaction of ionizing particles with this target volume is always a stochastic process. In this work, LET is considered as "unrestricted," which means that it accounts for the total kinetic energies of the electrons released in the collision of the charged particle. The correlation between LET and RBE is widely discussed in Part I. Microdosimetry is that part of radiation physics that deals with the stochastic analysis of the energy imparted by an ionizing particle to a sample of finite size [4]. An illustration of the stochastic nature of the energy imparted is provided in the next paragraph and in **Figure 1**. When the sample has the material composition and the size of a living cell or of one of its substructures, microdosimetry describes the primary radiation effect on the biological structure corresponding to that size, i.e., the living cell. Operative physical quantities are defined, which can be measured with special nuclear detectors called microdosimeters; International Commission on Radiation Units and Measurements (ICRU) Report 36 on Microdosimetry [4] and "Microdosimetry: Experimental Methods and Applications"

[6] are general references for the detailed description of the quantities and comprehensive formalisms.

In the following, a summary is given of the state of the art of studies aimed to investigate the use the microdosimeters as LET and RBE monitors in therapeutic proton and carbon ion beams.

THE PHYSICAL BASE OF THE RADIATION ACTION ON HUMAN CELLS

In **Figure 2**, RBE_{10} data are plotted against *LET* values of protons and carbon ions [7]. In order to produce these radiobiological data, monolayers of human cells were irradiated with mono-energetic protons and carbon ions, the *LET* value of which was calculated. Different *LET* values were obtained by changing the ion energy. Radiobiological measurements usually have a precision of about 10% when performed by the same research group. However, data in **Figure 2** show higher *RBE* fluctuations, since they originate from different experimental scenarios. In addition, while substantial uncertainties on *RBE* are widely acknowledged, there may be uncertainties as high as 15% in the consistency of the calculation of *LET* [8]. Without a significant reduction of the uncertainties, it is difficult to assess whether or not the RBE is a unique function of *LET*, independent of particle type. **Figure 2** shows clearly that, to a first approximation and within uncertainties, the *RBE* can be described as a function of *LET*: it increases with the *LET* value up to about 150 keV/μm, then it decreases likely because of damage saturation at high *LET* values. However, some experimental data are not consistent with the unique dependence of *RBE* on *LET* [9], pushing the researcher to deeper study of the physical basis of the biological action of radiation. As discussed in detail in Part I in the section "Accuracy of LET_D as Descriptor for RBE," there is indeed a general awareness that the biological effect depends, rather than on *LET*, on the density of energy imparted by a single particle to a biological structure, which is of fundamental importance for the cell surviving. The size of the relevant biological volume *V* might be as large as the cell itself (∼10 μm of thickness) or smaller as a chromosome (about 1 μm of thickness) or as small as the DNA strand (2 nm of thickness). The *energy imparted* is called ε. The energy imparted by a single particle is indicated using the subscript 1 (ε_1). Its linear density is called lineal energy and defined as:

$$\mathbf{y} = \frac{\varepsilon_1}{\bar{l}} \qquad (1)$$

where $\bar{l}$ is the biological site's mean-path length of primary tracks. The value of $\bar{l}$ is assessed, *via* calculations or simulations, considering the distribution of the actual paths of the particles in the sensitive volume, which depend on the track directions and the shape of the site. In equation (1), the *path length* (the term follows the nomenclature suggested by Bolst et al. [10]) substitutes the *chord length* used in the definition of lineal energy given in the ICRU Report 36 [4] and ICRU Report 85 [11]. In the original definition, $\bar{l}$ is specified for μ-randomness as described by Kellerer [12] and is independent on the beam direction. As an example, the mean chord length of a sphere
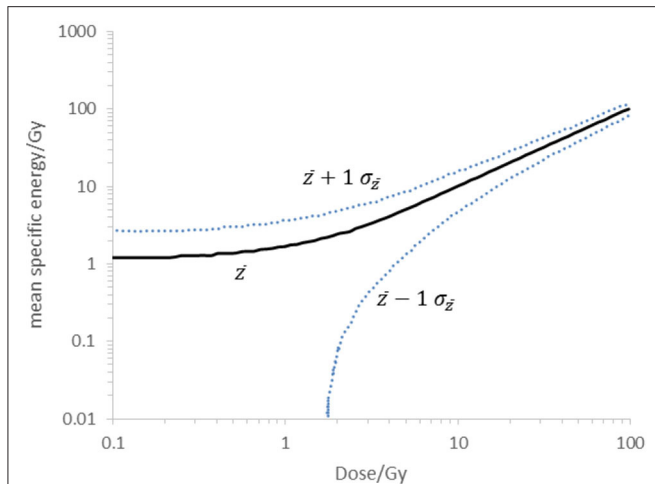
FIGURE 1 | Multi-event mean specific energy in a critical cylindrical volume of 1 μm in diameter (volume without 0 events) at a given dose, D. Calculation for a 60 MeV modulated proton beam at the Bragg peak with $y_F = 7$ keV·μm^{-1} and $y_D = 7$ keV·μm^{-1} (solid line). The dotted lines indicate the borders of the specific energy within 1 SD of the mean value in the actual energy distribution. Calculation was performed following the method described by Booz [5].
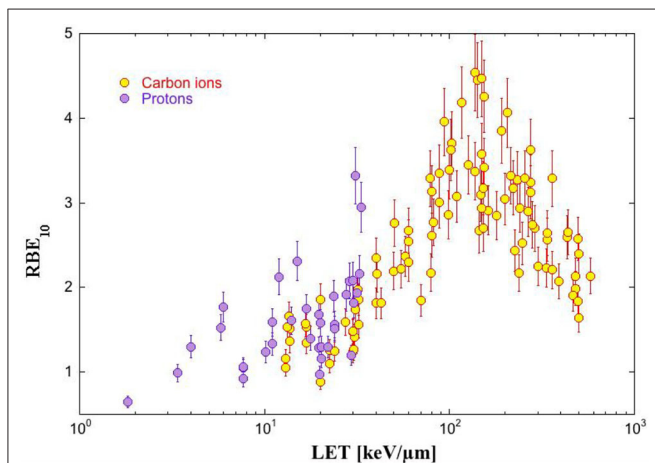

FIGURE 2 | Relative biological effectiveness (**RBE**) for asynchronous radioresistant human cell (different cell lines) after irradiation with protons and carbon ions is plotted against the particle linear energy transfer (**LET**) in tissue. The **RBE**$_{10}$ means that the **RBE** values have been taken at 10% of cell surviving fraction. Data from Friedrich et al. [7].

corresponds to 4/3 of its radius. The choice made for equation (1) of substituting the mean path length to the mean chord length is done since this quantity is more representative of the local density of energy imparted.

The unusual term "lineal energy" was adopted to remember the specific physical nature of y, which is, differently from **LET**, a stochastic quantity. In fact, ε_1 is a stochastic quantity too, since its value changes every time new particles interact with the cell, even if the particle type and initial energy are the same. This results from the non-deterministic nature of the atomic and nuclear

processes. Therefore, repeated measurements of y give rise to a spectrum of values indicated by the probability density function $f(y)$. The average obtained from $f(y)$ is called *frequency mean* of y, and it is written as $\bar{y}_F$:

$$\bar{y}_F = \int y \cdot f(y) dy \tag{2}$$

In microdosimetry, the specific energy z is defined as follows:

$$\mathbf{z} = \frac{\varepsilon}{m} \tag{3}$$

where m is the mass of V. **Figure 1** illustrates the stochastic nature of the energy imparted in a site size of 1 μm for a proton beam at the Bragg peak. The specific energy spectrum might exhibit a very broad width related to a site of about 1 μm size. As an example, the mean specific energy and the lines characterizing ± 1 SD of the spectrum at different dose levels are indicated in **Figure 1**. In this example, for the dose of 2 Gy, the specific energies in the micrometric site range between the values of 0.7 and 4.7 Gy, within 1 SD to the mean value.

The specific energy of a single event is written z_1 and is proportional to y:

$$\mathbf{z_1} = \mathbf{y} \frac{\bar{l}}{\mathbf{m}} \tag{4}$$

Repeated measurements of z_1 give rise to a spectrum of values, the average of which is called *frequency mean* of z_1 and is denoted $\bar{z}_{1F}$.

The microdosimetric spectrum represented by $f(y)$ indicates the probability to have, in V, an event with lineal energy y or specific energy z_1. The y or z_1 spectra display the stochastic behavior of these quantities, as well as the heterogeneity of the types and energies of the particles crossing the detector. Note that the microdosimetric spectrum of a particle depends on the size and shape of V, as well as on the radiation field anisotropy. Therefore, the same mono-energetic ion beam may give rise to different microdosimetric spectra in volumes of different sizes. Effects of a specific path length distribution on the measured microdosimetric spectrum can be studied through Monte Carlo simulations and mathematical models [13].

MICRODOSIMETRIC DETECTORS

Microdosimetric detectors can be based on gas counters or on solid-state counters (SSD). The first microdosimeters were gas proportional counters made with tissue-equivalent plastic and filled with tissue-equivalent gas mixtures. Because of that, they were called tissue-equivalent proportional counters (TEPCs). Miniaturized TEPCs (mini-TEPCs) with sensitive volumes of <1 mm have been manufactured in order to be operable in high-intensity therapeutic ion beams [14] (**Figure 3**). The simulated site size is determined by adjusting the gas density, so that the same amount of energy is imparted to the gas cavity as for the simulated volume of biological tissue. The energy imparted to a spherical cavity with a diameter of 1 mm and filled at about half

of atmospheric pressure is equivalent to the energy imparted to a 1-μm sphere of tissue, the density of which is 1 g/cm^3. Therefore, it is customary to say that the sensitive volume of the mini-TEPC simulates 1 μm of tissue. However, mini-TEPCs can simulate different site sizes by changing the gas pressure. Mini-TEPCs operate in the range from about 0.3 to 2 μm.

The silicon telescope is a detector used in nuclear physics to detect every single ion emerging from a nuclear reaction. The telescope idea has been exploited to manufacture a microdosimeter, where the 2-μm ΔE stage is the sensitive volume and the E stage is used to determine charge and energy of the ions. A scaling factor can be applied to convert ε_1 in silicon to ε_1 in tissue [13] (**Figure 3**). The non-tissue-equivalence of silicon is dealt with by using, as scaling factor for the energy imparted, the ratio of the electronic stopping power in tissue and in silicon. Furthermore, a shape equivalence correction is applied to compare spectra obtained with detector sensitive volumes of different shapes. Other silicon counters have been developed and are nowadays on the market with the name of MicroPlus Bridge [15] (**Figure 4**). These detectors, unlike silicon telescopes, are formed by a single thin layer and provide different settings as matrixes of detectors with different cross sections and thicknesses [16]. The so-called "Mushroom" version features a 50×50 matrix of cylindrical sensitive volumes with thicknesses that range between 2 and 10 μm and diameter of 18 μm [17]. Microdosimeters based on Schottky diode and made of synthetic diamond of thickness varying from 0.3 to 10 μm have been manufactured as well [18] (**Figure 4**).

TEPCs have high detection efficiency, since they can detect also few ionization events—thanks to the electron multiplication in the filling gas. However, the electrodes are biased at several hundreds of volts, they need accurate gas pressure control and energy calibration, and they have limited capabilities in high-intensity radiation fields because the geometrical cross-sectional area of the sensitive volume can hardly be reduced below 1 mm^2. Solid-state microdosimeters have lower detection efficiency because they rely on the collection of the free charges generated in the sensitive volume not taking advantage of internal charge amplification. On the other side, they are biased at low voltage and the thickness of the sensitive volume can be as small as 1 μm, making them suitable for operation even in very intense radiation fields. Moreover, pixelated arrays of detectors can be constructed, allowing the simultaneous two-dimensional mapping of the radiation field.

It is worth underlining that microdosimetry measures the probability distribution of the energy deposit ε_1, which obviously depends on the radiation field properties but also on the composition, size, and shape of the sensitive volume. Therefore, detectors that differ in material composition, size, and shape might be measuring different microdosimetric distributions, according to their specific response function.

All the microdosimeters described above estimate the energy imparted by measuring the free charges produced in the medium and then converting the number of those measured charges to energy imparted through the multiplication by the W-value, the mean energy expended to form an ion pair. W-value for different

particles is not constant. It increases for higher Z-ions, resulting in additional uncertainty.

An interesting conceptual design has been proposed for a microcalorimeter that measures directly the energy imparted rather than the ionization [19]. The realization of such a detector is however a great challenge. In particular, the definition of the thermal behavior of this detector is complex. The goal is to determine the radiation-induced temperature increase in a tissue-equivalent absorber while the temperature measurement is performed on the superconductor, which is in thermal contact with the absorber. Fathi et al. [20] discussed this topic proposing a correction of the microdosimetric spectra from microcalorimeters. Another major challenge for the realization of microdosimeters based on microcalorimetry is the difficulty in translating a cryogenic detection to a clinical environment.
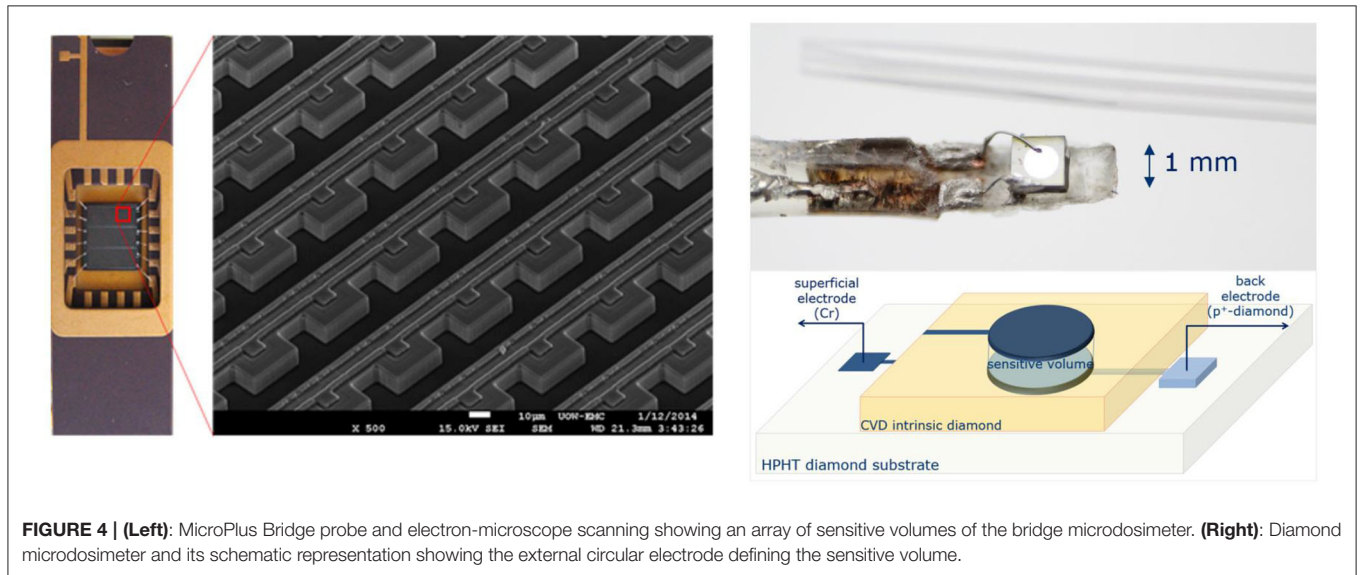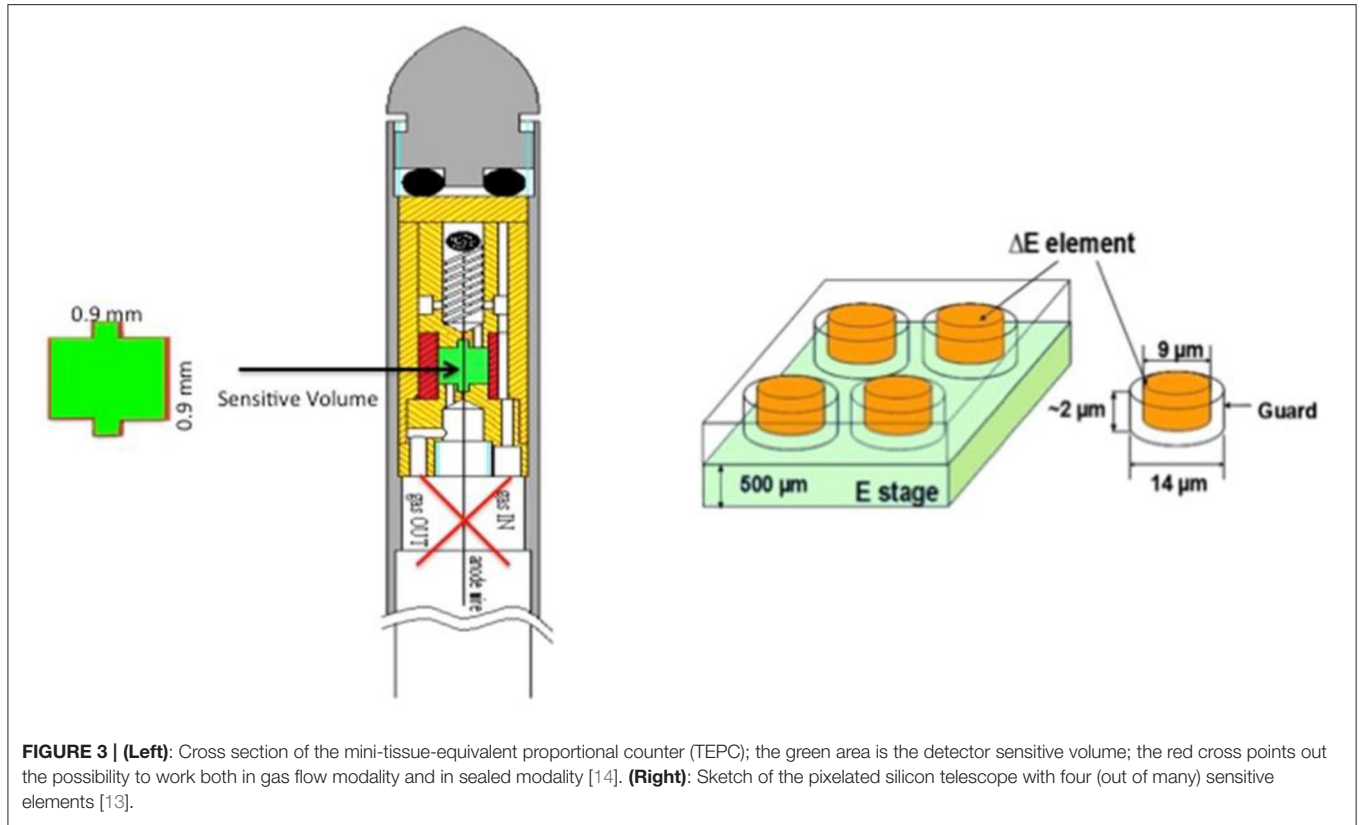
Other prototypes of microdosimeters have been studied and developed to be used in ion-beam therapy including TEPCs [21], solid state detectors [22, 23], gas electron multiplier (GEM) detectors [24], and films [25].

ASSESSING VARIATIONS OF LINEAR ENERGY TRANSFER IN PROTON DATA

As is discussed in the section "Basic Concepts of Models" of Part I, in proton therapy, a constant $RBE = 1.1$ is assumed along the entire spread-out Bragg peak (SOBP). However, radiobiological data show that the proton RBE at the end of the range is more than twice the RBE value at the entrance [26] and thus the choice of a constant value is questionable. This finding is consistent with the radiobiological data of **Figure 2** if we consider that the proton LET value at the end of a proton track in tissue is about 85 keV/μm.

The current practice of proton therapy planning with a constant RBE of 1.1 is thus questionable. As a first step, several treatment planning systems (TPS) are already offering the possibility to take the LET variation along the penetration depth into account. In view of the implementation of LET-based treatment planning systems, it is necessary to develop tools and methods for the quality assurance of LET determination and calculation. Microdosimetry could offer valuable tools for that purpose [27].

The frequency mean lineal energy has the same physical dimensions as LET, but not necessarily the same value. In fact, the LET is defined at a point for a mono-energetic ion beam [28]; therefore, its value does not depend on V. Conversely, $\bar{y}_F$ does not include the energy transported outside the volume V by fast electrons or secondary ions (it averages only the ε_1 events occurring inside V). Moreover, $\bar{y}_F$ automatically averages the y values due to ions of different energies and of different types. This last feature makes microdosimeters suitable to measure the mean lineal energy density in a mixed radiation field like that one of therapeutic ion beams. Therefore, as far as $\bar{y}_F$ can substitute the LET, the mean RBE_{10} values of **Figure 2** can be represented as a function of the frequency mean lineal energy. A similar figure can be obtained for RBE, which are therapeutically significant

FIGURE 3 | (Left): Cross section of the mini-tissue-equivalent proportional counter (TEPC); the green area is the detector sensitive volume; the red cross points out the possibility to work both in gas flow modality and in sealed modality [14]. **(Right)**: Sketch of the pixelated silicon telescope with four (out of many) sensitive elements [13].

FIGURE 4 | (Left): MicroPlus Bridge probe and electron-microscope scanning showing an array of sensitive volumes of the bridge microdosimeter. **(Right)**: Diamond microdosimeter and its schematic representation showing the external circular electrode defining the sensitive volume.

and can be used by clinicians to adapt the absorbed dose data in therapeutic plans. This process would result in a decrease of the absorbed dose at distal depths.

The dose distribution $d(y)$ is calculates as:

$$d(y) = \frac{y \cdot f(y)}{\bar{y}_F} \qquad (5)$$

In mixed radiation fields, the dose weighted distribution is frequently preferred to $f(y)$ because dose weighted quantities, e.g., the dose-averaged LET ($\overline{LET}_D$), better correlate to the radiobiological effectiveness. The mean value of y weighted by $d(y)$ is called the dose mean lineal energy:waker

$$\bar{y}_D = \int y \cdot d(y) dy \qquad (6)$$

FIGURE 5 | Typical microdosimetric spectrum collected using a tissue-equivalent proportional counter (TEPC) in a proton beam. The two vertical lines represent the mean values $\bar{y}_F$ and $\bar{y}_D$ estimated from the spectrum.
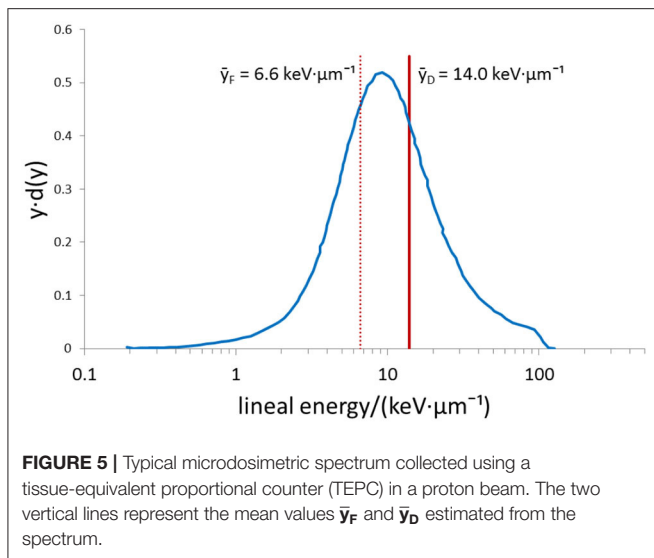
(See also in Part I the section "Role of the Microscopic Energy Deposition Pattern"). A typical microdosimetric spectrum of a proton beam collected with TEPC and the corresponding mean values are presented in **Figure 5**. Also this quantity has the same physical dimensions of *LET*, its meaning being the mean *y* value of events that contribute to the absorbed dose. The correspondence between measured $\bar{y}_D$ values and calculated $\overline{LET_D}$ values must be studied and characterized. Afterward, microdosimetric characterization in terms of $\bar{y}_D$ can be used for the quality assurance of *LET*-based treatment plans [27].

Data of **Figure 6** (taken from Conte [29]), show two sets of $\bar{y}_D$ values (taken with the mini-TEPC in two separate shifts of measurements) compared with $\overline{LET_D}$ values simulated with Geant4 Monte Carlo code with energy imparted in the same tissue equivalent sensitive volume size $1.0\,\mu\text{m}$ as in used TEPC. They suggest that microdosimeters could be accurate *LET* monitors, given that the difference between the two sets of values is <5% [32].

THE MICRODOSIMETER AS RELATIVE BIOLOGICAL EFFECTIVENESS MONITOR

Another possibility is to use the peculiarity of the radiobiological microdosimetric model to directly monitor the *RBE*.

The microdosimetric model assumes that, as far as biological effects of radiation are concerned, the radiation quality (physical) can be adequately characterized by the probability distribution of lineal energy in a sensitive site representative of the biological target that is supposed to be critical for the biological observable. The *y* distribution measured by a microdosimeter is considered equal to the *y* distribution in the biological site if the detector sensitive volume is tissue-equivalent and its size, calculated at a density of 1 g·cm^{-3}, is the same as that of the critical biological site. The model is sketched in

Figure 7 where the analogy between the measured *y* events and *y* events experienced by chromosomes is presented. The microdosimetric spectrum represents in fact all the possible y values occurring in the cell chromosome at the passage of one ionizing particle.

Since the mean effect (for a given radiation field, cellular target, and biological end point) of an ion impinging on a living cell is expected to be always the same, while $\bar{y}_F$, and $\bar{y}_D$ depend on *V*, it is legitimate to ask oneself whether the value of *V* has a radiobiological meaning (e.g., if the size of *V* can be really interpreted as the size of the "critical" living cell structure, like the heart of a human being). If the critical site really existed, the microdosimetric spectrum in that volume *V* would likely be stronger correlated to radiobiological data than microdosimetric spectra in volumes of different sizes. As discussed in Part I in the section "Role of the Microscopic Energy Deposition Pattern," an important aspect that needs to be considered is that multiple volume sizes are relevant with respect to different biological pathways to cell damage and thus that a multiscale characterization is needed for a full description of the relation between the physical energy deposition and the biological effect [33].

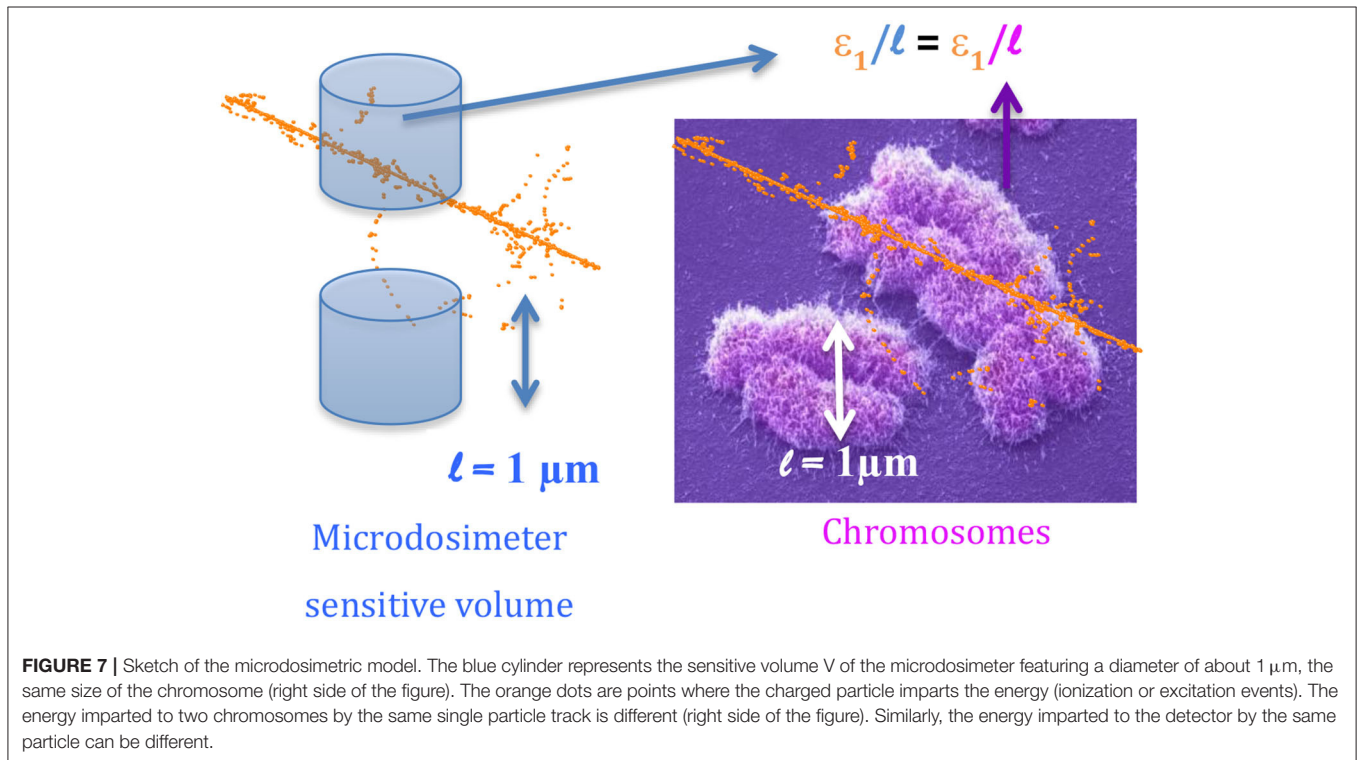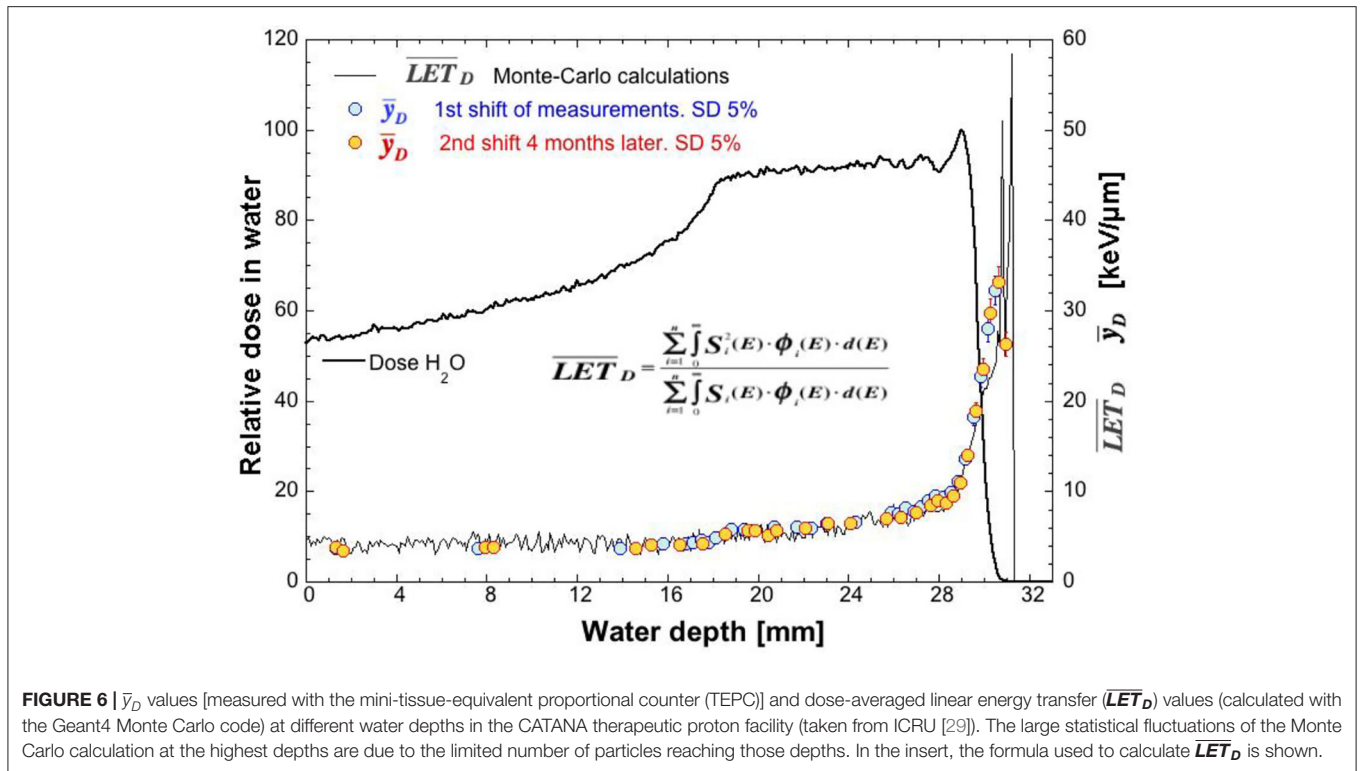## THE MICRODOSIMETER TO MONITOR RELATIVE BIOLOGICAL EFFECTIVENESS, PROTON DATA

The $\bar{y}_D$ value cannot directly mimic the *RBE* for the simple reason that its value increases always with the ion *LET* value. Instead, the *RBE* value reaches a maximum and then it decreases (**Figure 2**), since after the destruction of the biological target, a further increase of linear energy-deposition density (which corresponds also to an increase of the proton dose) cannot contribute to any additional effects.

A possibility to simulate the "saturation effect" that appears in **Figure 2** is to "weigh" the *d(y)* spectrum with a biological response function *r(y)*, which represents the expected biological effect due to the dose component with lineal energy *y*. The *RBE* microdosimetric assessment, which is called *RBE*$_{\text{micros}}$, would therefore be:

$$\text{RBE}_{\text{micros}} = \int_{y_{\text{min}}}^{y_{\text{max}}} r(y) \cdot d(y) \cdot dy \tag{7}$$

A successful *r(y)* function was extracted from the experimental comparison of *TEPC* microdosimetric spectra in 2-μm tissue-equivalent sites in photon, proton, and fast neutron beams and the *RBE* for crypt cell regeneration after 8 Gy of dose on living rats exposed to the same beams [34–36]. The determination of the biological effectiveness on mouse crypt cells for the characterization of clinical proton beam has been widely discussed and applied [26, 37–43]; With such a response function, the *RBE*$_{\text{micros}}$ values of the Nice therapeutic proton beam are able to monitor the specific *RBE* value with good accuracy [44].

In **Figure 8**, the plot representing the dependence of *RBE*$_{10}$ on *LET* (from **Figure 2**) is superimposed on the plot of *RBE*$_{\text{micros}}$

FIGURE 6 | $\bar{y}_D$ values [measured with the mini-tissue-equivalent proportional counter (TEPC)] and dose-averaged linear energy transfer ($\overline{LET}_D$) values (calculated with the Geant4 Monte Carlo code) at different water depths in the CATANA therapeutic proton facility (taken from ICRU [29]). The large statistical fluctuations of the Monte Carlo calculation at the highest depths are due to the limited number of particles reaching those depths. In the insert, the formula used to calculate $\overline{LET}_D$ is shown.

FIGURE 7 | Sketch of the microdosimetric model. The blue cylinder represents the sensitive volume V of the microdosimeter featuring a diameter of about 1 μm, the same size of the chromosome (right side of the figure). The orange dots are points where the charged particle imparts the energy (ionization or excitation events). The energy imparted to two chromosomes by the same single particle track is different (right side of the figure). Similarly, the energy imparted to the detector by the same particle can be different.

data vs. the microdosimetric mean $\bar{y}_D$ values measured at the CATANA therapeutic proton beam. Microdosimetric values follow rather well the linear best fit of radiobiological data

(red line). These findings suggest that microdosimetric spectra in a volume V of about 1 μm of tissue-equivalent thickness can be used to simulate the dependence of RBE on LET
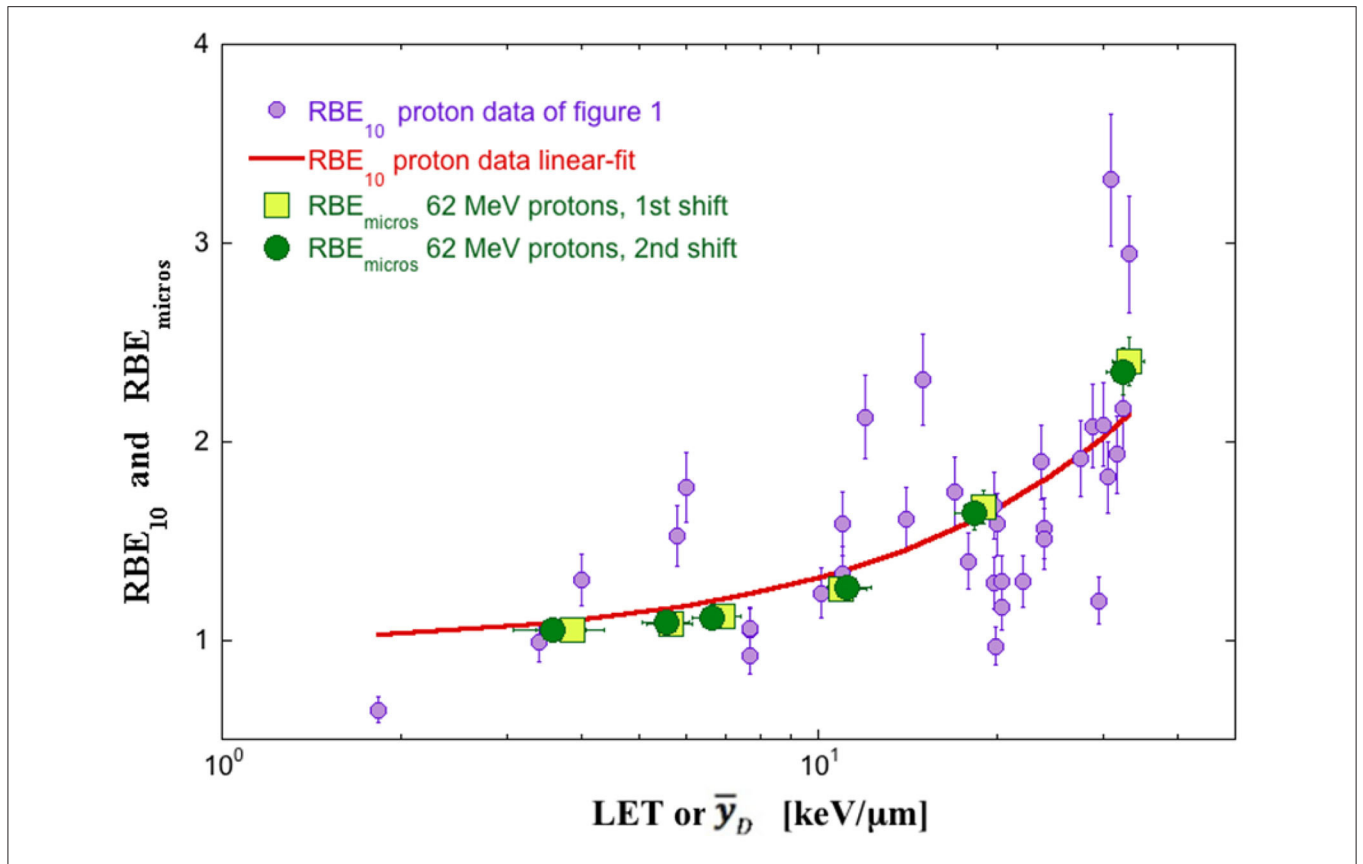
FIGURE 8 | The relative biological effectiveness microdosimetric assessment (**RBE$_{micros}$**) (squares and circles) vs. measured $\overline{y}_D$ [mini-tissue-equivalent proportional counter (TEPC) measurements in 1-μm site at the 62 MeV proton beam of CATANA] and **RBE$_{10}$** (violet circles) vs. calculated linear energy transfer (**LET**) values. The red line is the linear best fit of **RBE$_{10}$** data. Squares and circles point out two different shifts of measurements 4 months apart. Data from ICRU [29].
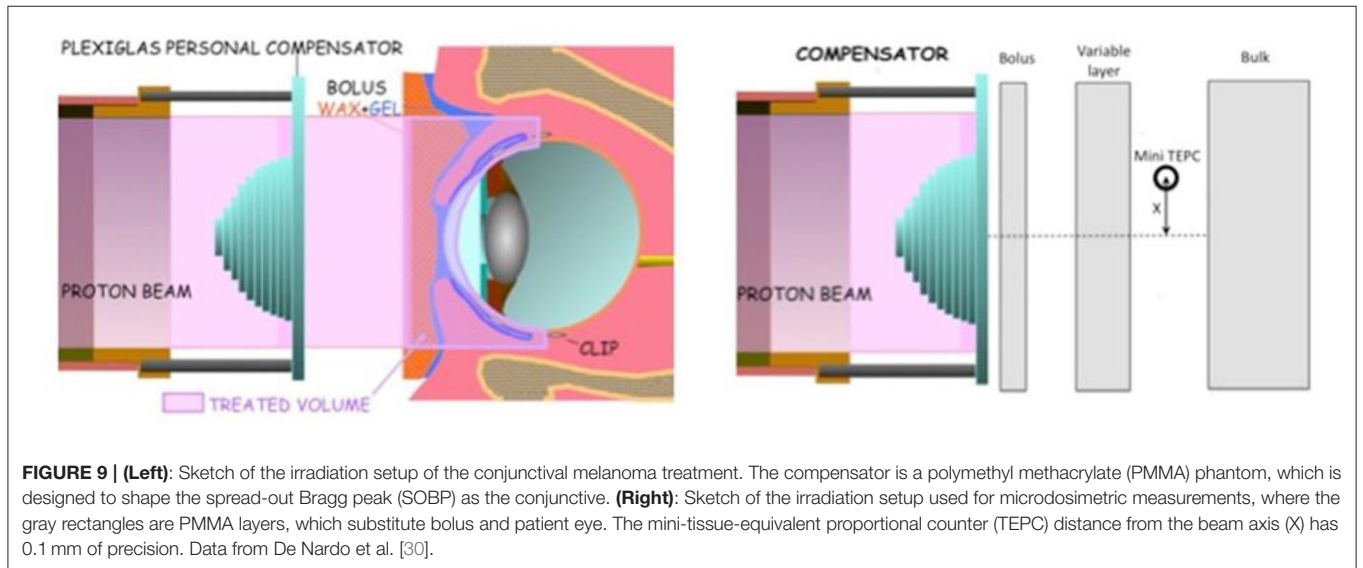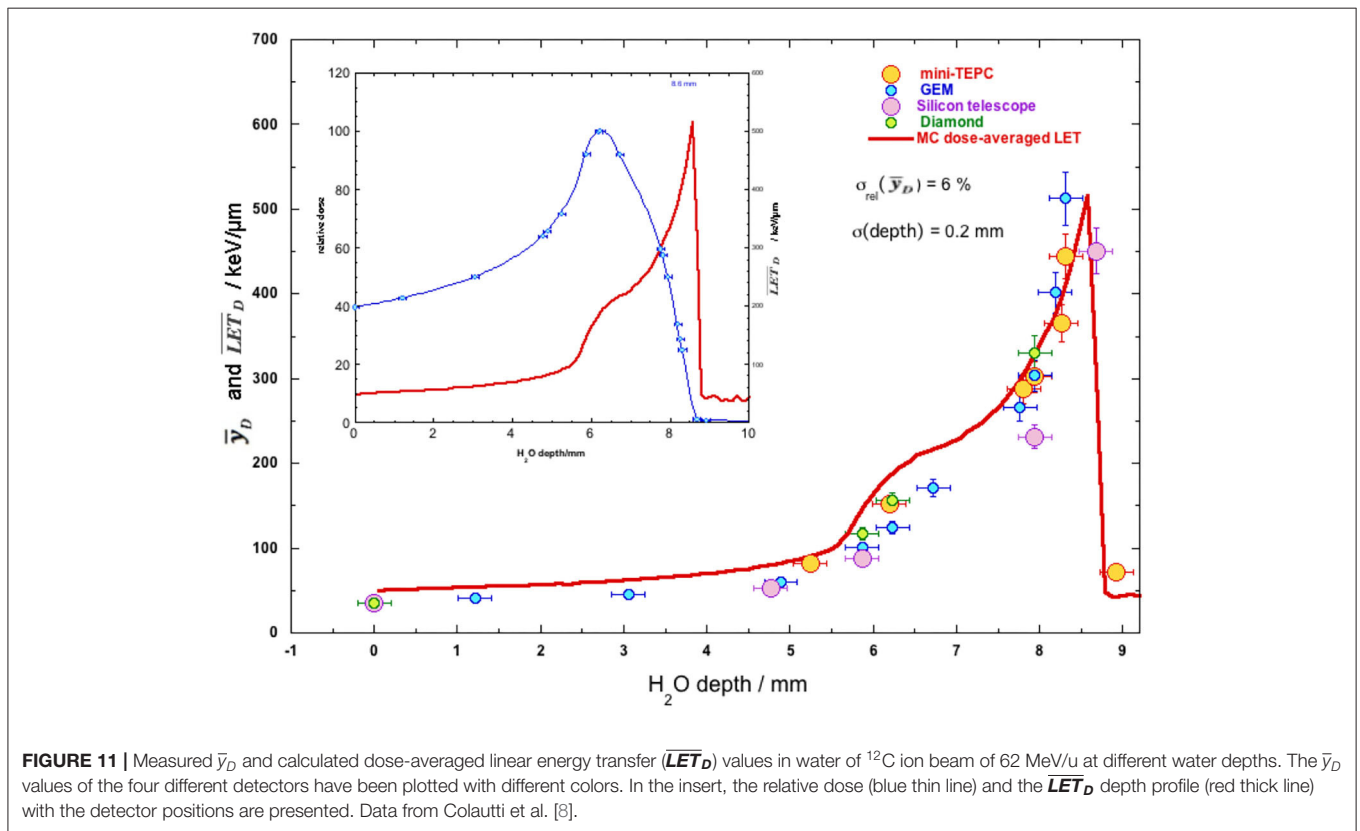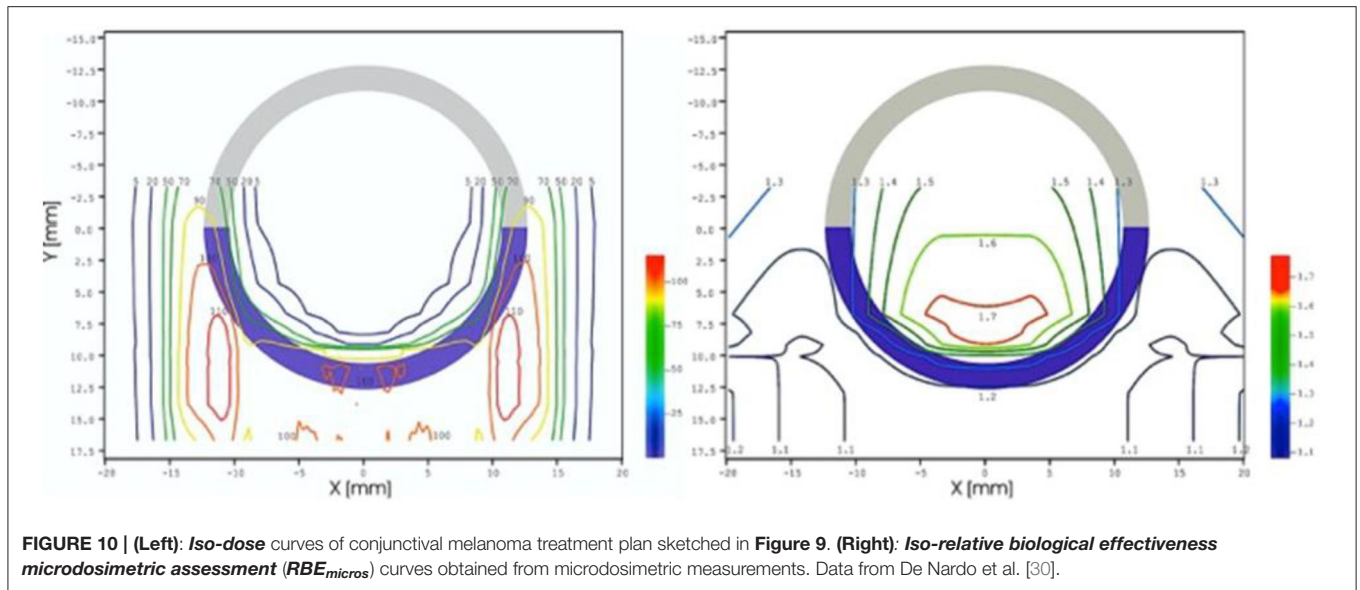

FIGURE 9 | (Left): Sketch of the irradiation setup of the conjunctival melanoma treatment. The compensator is a polymethyl methacrylate (PMMA) phantom, which is designed to shape the spread-out Bragg peak (SOBP) as the conjunctive. **(Right)**: Sketch of the irradiation setup used for microdosimetric measurements, where the gray rectangles are PMMA layers, which substitute bolus and patient eye. The mini-tissue-equivalent proportional counter (TEPC) distance from the beam axis (X) has 0.1 mm of precision. Data from De Nardo et al. [30].

for crypt cell regeneration in living rats with an accuracy of about 5%. New weighting functions $r(y)$ can be unfolded for other specific bi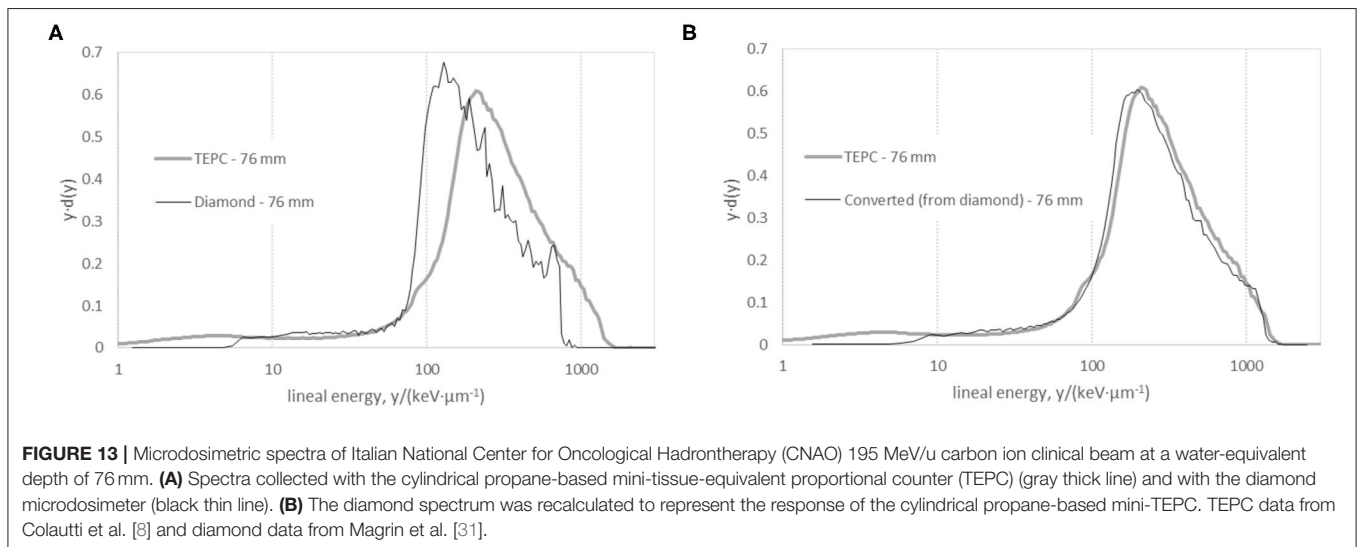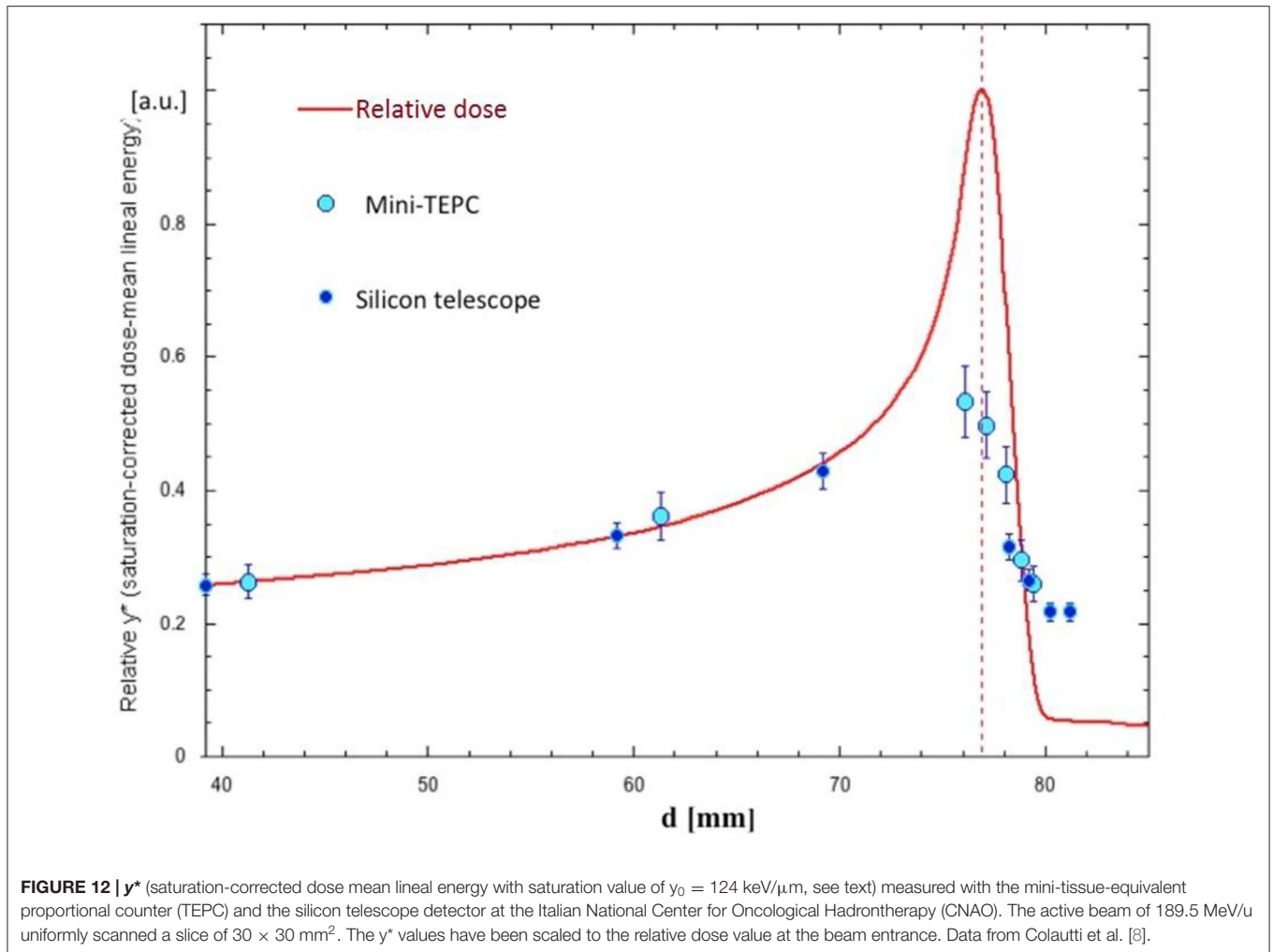ological endpoints and using microdosimetric spectra collected with other detector types to provide, through equation (7), specific insights on the **RBE** of the tumor and healthy tissue.

FIGURE 10 | (Left): *Iso-dose* curves of conjunctival melanoma treatment plan sketched in **Figure 9**. **(Right)**: *Iso-relative biological effectiveness microdosimetric assessment* (RBE_{micros}) curves obtained from microdosimetric measurements. Data from De Nardo et al. [30].

FIGURE 11 | Measured $\bar{y}_D$ and calculated dose-averaged linear energy transfer ($\overline{LET}_D$) values in water of ^{12}C ion beam of 62 MeV/u at different water depths. The $\bar{y}_D$ values of the four different detectors have been plotted with different colors. In the insert, the relative dose (blue thin line) and the $\overline{LET}_D$ depth profile (red thick line) with the detector positions are presented. Data from Colautti et al. [8].

HOW TO USE RELATIVE BIOLOGICAL EFFECTIVENESS MICRODOSIMETRIC ASSESSMENT VALUES IN A THERAPEUTIC PLAN: AN EXAMPLE

The conjunctival melanoma is a rare tumor (3% of all ocular melanomas), which is difficult to treat with success by using conventional radiotherapy. At the Center Antoine Lacassagne in Nice (France), the 65 MeV proton beam provided by the MEDICYC cyclotron is used to treat the conjunctival melanoma. However, the complexity of the irradiation (see left side of **Figure 9**), which uses a hemispherical polymethyl methacrylate (PMMA) plastic, compensator, raises questions about the

FIGURE 12 | y^* (saturation-corrected dose mean lineal energy with saturation value of $y_0 = 124$ keV/μm, see text) measured with the mini-tissue-equivalent proportional counter (TEPC) and the silicon telescope detector at the Italian National Center for Oncological Hadrontherapy (CNAO). The active beam of 189.5 MeV/u uniformly scanned a slice of 30 × 30 mm². The y* values have been scaled to the relative dose value at the beam entrance. Data from Colautti et al. [8].

FIGURE 13 | Microdosimetric spectra of Italian National Center for Oncological Hadrontherapy (CNAO) 195 MeV/u carbon ion clinical beam at a water-equivalent depth of 76 mm. (A) Spectra collected with the cylindrical propane-based mini-tissue-equivalent proportional counter (TEPC) (gray thick line) and with the diamond microdosimeter (black thin line). (B) The diamond spectrum was recalculated to represent the response of the cylindrical propane-based mini-TEPC. TEPC data from Colautti et al. [8] and diamond data from Magrin et al. [31].

variability of radiation quality across the conjunctiva. To answer these questions, a microdosimetric approach was used.

The patient irradiation setup was simulated with a PMMA phantom, the compensator being the same as the one used for treatment (see right side of **Figure 9**). Microdosimetric spectra

were measured with a mini-TEPC placed at different lateral distances from the proton beam axis.

In the left side of **Figure 10**, the iso-dose curves of the traditional treatment plan are plotted, while in the right side of the figure, the iso-RBE_{micros} curves are plotted. The iso-RBE_{micros} curves are obtained using the RBE_{micros} values calculated from equation (7) at the different positions.

Microdosimetric data show that RBE_{micros} is almost invariant with value between 1.2 and 1.3 throughout all of the conjunctiva. In this experimental example, microdosimetric measurements confirmed the goodness of the treatment plan. The results of **Figure 10** show how to implement an "upgraded" treatment plan, which includes RBE_{micros} data.

MICRODOSIMETRIC MONITORING OF THERAPEUTIC CARBON ION BEAMS

Figure 2 shows clearly that carbon ions reach a biological effectiveness higher than protons at the end of the track, where the LET values are in the range 100–200 keV/μm. The increase of RBE at the end of the carbon ion range is one main factor that justifies the high cost and complexity of the particle accelerators that are necessary to accelerate the ions up to the energy necessary to treat deep-seated tumors (∼5 GeV). Therefore, in carbon ion therapy, the RBE variation with depth in the irradiated tissue must be taken into account when optimizing a treatment plan (in order to maximize the tumor control probability and minimize the normal tissue complications probability). Considering the complexity of the radiation field produced by carbon ions inside the patient body, the microdososimetric characterization is a useful experimental tool. Complementary to models that describe the radiation biological action, microdosimeters can be used to monitor LET, RBE_{10}. More generally, microdosimeters might serve as an instrumental support to improve the comparison among different radiation centers concerning therapeutic gain.

The Microdosimeter to Monitor Linear Energy Transfer, Carbon Ion Data

In the section Assessing Variations of Linear Energy Transfer in Proton Data, the advantages and the disadvantages of some current microdosimeters have been presented, the main drawback of solid-state detectors being the relatively high detection threshold, which makes them less suited to monitor low LET radiation and in general the LET in therapeutic proton beams (**Figure 6**). The discriminator level of the solid-state detectors depends on the thickness of the sensitive volume. The silicon and diamond detectors described in the section Microdosimetric Detectors with physical thickness of ∼2 μm have a discrimination level just below 10 keV·μm^{-1} [13, 18]. When the thickness is increased to 10 μm, the discrimination level decreases to about 2 keV·μm^{-1} for diamond detectors and 0.2 keV·μm^{-1} for the MicroPlus/Mushroom detectors [15]. The low sensitivity limits are less severe with carbon ions, since microdosimetric spectra shift toward higher values and show low contributions from small y-values.

In order to test the capability of different detectors to monitor the $\overline{LET}_D$ of carbon ion beams, four different microdosimeters (the mini-TEPC, the silicon telescope, the diamond microdosimeter described in the section The Microdosimeter as Relative Biological Effectiveness Monitor, and a multi-element gas counter with GEM technology [45]) have been exposed to the same carbon ion beam of 62 MeV/u [8]. In **Figure 11**, the $\overline{y}_D$ values measured at different depths in a water-equivalent phantom are plotted together with the $\overline{LET}_D$ values calculated with the Geant4 Monte Carlo code (see the inserted algorithm in **Figure 6**). The figure shows that, in spite of the detectors' differences, the $\overline{y}_D$ values are very similar, the relative standard deviation of the mean of all the data being 15%. Part of this variance is certainly due to the detector position uncertainty. Therefore, all the microdosimeters are able to monitor the calculated $\overline{LET}_D$ as $\overline{LET}_D = k \cdot \overline{y}_D$, where the proportionality factor k depends on the beam anisotropy as well as on the detector's angular response. For instance, k assumes the values of 1, and 1.08, for a unidirectional beam with the direction normal to the face of a slab detector and to the axis of a cylindrical detector, respectively. For spherical detectors, k is always 1.125, for isotropic as well as unidirectional beams. It should be studied for each therapeutic facility before using any microdosimeter as $\overline{LET}_D$ monitor.

A similar comparison was performed with the 195 MeV/u active carbon ion beam of the Italian National Center for Oncological Hadrontherapy (CNAO) in Pavia, Italy, by using the mini-TEPC and the diamond microdosimeter [31]. Also in this case, the $\mathbf{y}_D$ value differences are within 15% with a standard deviation of 6%, being mainly attributable to the detector position uncertainty in a radiation field, the microdosimetric quality of which changes rapidly with depth.

The Microdosimeter to Monitor Relative Biological Effectiveness, Carbon Ion Data

As far as $\overline{y}_D$ is able to properly monitor $\overline{LET}_D$, proportionality with the RBE_{10} cannot be assumed because of the saturation effect that results in the reduction of RBE at very high LET in **Figure 2**. The microdosimetric spectrum should be properly weighted, but the weighting function used for proton therapy discussed in the section The Microdosimeter to Monitor Relative Biological Effectiveness, Proton Data does not seem to work with carbon ions [46]. These differences arise from the distinct characteristics of the track structures of protons and carbon ions, also in the case of identical $\overline{LET}_D$. The section "Use of Focused Low-LET Proton Beams to Mimic High-LET" of Part I provides additional details. For carbon ion irradiation, the saturation effect can be introduced with the so-called "saturation-corrected dose mean lineal energy" or $y*$.

$$y* = \frac{y_0^2 \cdot \int [1 - e^{-\left(\frac{y}{y_0}\right)^2}] \cdot f(y) dy}{\int y \cdot f(y) dy} \tag{8}$$

where the free parameter y_0 is the y-value at which the biological effect saturates [4].

The ^{12}C therapeutic active beam of CNAO was used to derive y^* based on y measured with the mini-TEPC and the silicon telescope microdosimeter. **Figure 12** shows the very similar results obtained with the two detectors at different depths in a water phantom. As expected, the y^* value increases with the depth up to a maximum value and then it decreases mimicking the saturation effect of **Figure 2**.

The y^* value has been inserted in the microdosimetric kinetic model (MKM) (see Part I) to assess RBE_{10} of human salivary gland cells at the Heavy Ion Medical Accelerator in Chiba (HIMAC) therapeutic facility with a 290 MeV/u carbon ion beam. Measurements performed with a large TEPC (12.7 mm of diameter) are able to monitor the clinic biological dose with good accuracy [47]. The measurements have been repeated with the MicroPlus Bridge detector giving the same results, but in the distal edge where the large geometrical size of the TEPC could have compromised the position accuracy [48].

PROSPECTIVE OF MICRODOSIMETRY IN THE CLINICS

In carbon ion therapy, the passive beam spread modality used in the initial years to conform the radiation to the tumor targets has been gradually replaced by scanned beams [49]. The daily fraction is delivered to the patient from different portals and, for each portal, the pencil beam is scanned in three dimensions to thousands of different spot positions to cover the tumor target. Scanned carbon ion beams created new constraints and needs for experimental microdosimetry. Non-uniform distributions of the dose are feasible, and this is a feature used in the so-called "intensity modulated" therapy with ion beams. Thanks to the additional degrees of freedom, for each portal, the conformation of the irradiation can be adapted, optimizing the radiation quality across the target. Examples of these modalities are the "*LET*-painting" [50, 51] and the "Kill-painting" [52]. In these techniques, the radiation is delivered not only to preserve the dosimetric and the biological constraints but also to optimize the distribution of *LET* in the first case and to maintain uniform cell killing in volumes with heterogeneous radiosensitivity in the second case.

The complex radiation fields in these modalities show, inevitably, large *LET* gradients. In this scenario, the spectra collected with the microdosimeters in water phantoms can be used as radiation quality specifiers. The spatial density of the measurements can be increased where the LET gradient is higher or in the sub-volumes corresponding to critical, radiosensitive locations.

For carbon ion therapy beams, there are numerous microdosimetric data collected with a variety of detectors, gaseous and solid (a non-exhaustive selection is provided in the references [31, 46, 47, 53–55]). However, as discussed in the *Introduction*, the shape and material of the microdosimeters affect the experimental outcomes. To guarantee a univocal assessment of the radiation quality, the characteristics of the microdosimeters should be fixed. In particular, the "standards" for volume size, shape, aspect ratio, and the material to be used

as reference for the microdosimetric spectra should be defined and become the reference for all the different detectors.

An example of spectral conversion is shown in **Figure 13** and refers to data collected at 195 MeV/u carbon ion clinical beam of CNAO. It compares the spectrum collected with a propane-filled mini-TEPC [55] and the spectrum collected with a diamond microdosimeter and converted based on the shape and the material of the mini-TEPC [31]. The spectra conversion is the result of two successive conversion steps [56]. The first transforms the experimental spectrum collected with slab diamond detector to the spectrum that would be collected by a propane-filled slab detector using a function of the stopping powers of the two materials. The second conversion transforms the spectrum of the slab propane-filled detector to the spectrum that, for the same material, would be collected by a cylindrical detector, based on the path length distributions of the two shapes.

The experimental spectrum for the diamond detector is shifted toward lower lineal energies compared to the experimental spectrum collected with the propane-filled mini-TEPC (**Figure 13A**). This is due to two conditions. First, for the same particle energy, the energy imparted per unit of length and unit of mass is lower in diamond than in propane. Second, the maximum path length of a cylindrical detector is 27% higher than its mean path length (for irradiation normal to the cylinder axis) while, for a slab detector, maximum and mean path lengths coincide. This results in extending the spectrum of the cylindrical detectors toward higher lineal energy values.

Overall, after the conversion, the two spectra show a good agreement. The effect of the low sensitivity in solid-state detectors, discussed in the section Assessing Variations of Linear Energy Transfer in Proton Data, is visible in the diamond spectrum at lineal energies below 9 keV·μm^{-1}. A metrological approach needs to be established where univocal methodologies for the detector calibration and formalism for the representation of the spectra are implemented and shared among the users. This should include the uncertainty budget assessment of microdosimetric measurement performed with different tools and methods. The role played by Monte Carlo simulations in this process is discussed in the section Monte Carlo Codes in Microdosimetry.

It is worth mentioning here the work of Hagiwara et al. [57], indicating the potential value of microdosimetric data for the clinical outcome of ion beam therapy. In this clinical-based investigation, the outcomes of local control and overall survival in pancreatic tumors are assessed with retrospective studies and examined in relation to the dose mean *LET*. $\overline{LET_D}$ values are computed within the tumor volume and compared to the clinical outcome defined as lack of local control of tumor. The results show that the lowest value of $\overline{LET_D}$ within the tumor volume is a prognostic factor related to local failure. In all case studies, the 18-month local control was maintained at 100% when the minimum $\overline{LET_D}$ was maintained above 44 keV·μm^{-1}. In the plans where $\overline{LET_D}$ declines below 44 keV·μm^{-1}, the local control dropped to 34%. This is the example of a new paradigm in which the *LET* is explicitly taken into consideration for the outcome of the treatment, without the intermediate role of the RBE. As discussed in the section Microdosimetric Monitoring of

Therapeutic Carbon Ion Beams, microdosimetric spectra provide an estimate of **LET** in terms of track and dose mean values. However, the heterogeneity of the particle energies and species in different points of the target is not completely represented by single parameters, such as the averaged **LET**. Computations based on microdosimetric spectra, collected experimentally in complex phantoms, may provide a representation of the **LET** distributions. However, limited data are available yet for proving the accuracy of these derived **LET** distributions for complex phantoms and tissue structure.

The relevance of the measurement uncertainty of microdosimetric spectra and **LET** distributions with reference to the uncertainties of the biological outcome and clinical factors is still unclear. Furthermore, the environment surrounding the tumor may play an important factor. Investigating this should be part of the metrological approach suggested above. Note that the uncertainties on microdosimetric quantities, although smaller, may not be negligible compared to the biological uncertainties, contrary to the uncertainty of macroscopically measured absorbed dose to water. The spread of experimental data that relate biological to physical quantities may be determined not only by the substantial uncertainties of the biological data but also by the physical quantities at a microscopic scale. Monte Carlo simulations are a well-suited tool to aid establishing this uncertainty propagation chain.

MONTE CARLO CODES IN MICRODOSIMETRY

Radiation transport Monte Carlo codes have become frequent tools in microdosimetry research from both a theoretical and an experimental approach. In the last years, general-purpose Monte Carlo codes, such as FLUKA [58], Geant4 [59–61], and PHITS [62], have been used to verify the experimental outcomes, in which case it is key to include an appropriate modeling of the detector response [63, 64].

With properly validated interaction models, Monte Carlo simulations give a reliable benchmark to experimental data obtained with either TEPC or solid-state microdosimeters (see the sections The Microdosimeter as Relative Biological Effectiveness Monitor and The Microdosimeter to Monitor Linear Energy Transfer, Carbon Ion Data) [29, 65–67]. As indicated in the section The Physical Base of the Radiation Action on Human Cells, it is possible to evaluate the influence of specific path length distributions on the measured microdosimetric spectra by means of Monte Carlo simulation. The mixed radiation field properties can be evaluated by Monte Carlo simulations, and thus the contribution of each secondary ion can be quantified and be used as a reference to interpret the experimental microdosimetric spectra [68, 69]. These determinations can also help to evaluate correction factors to convert microdosimetric quantities measured in solid-state microdosimeters to equivalent ones in tissue (see the section Prospective of Microdosimetry in the Clinics) [10]. Also, as indicated in the section Assessing Variations of Linear Energy Transfer

in Proton Data, Monte Carlo simulations constitute a powerful tool for the design phase of new concepts of microdosimetry detectors, as sensitivity analysis can be carried out with numerical simulations, saving costs [70]. Microdosimetry calculations have been used as a benchmark to define a method suitable for scoring $\overline{LET_D}$ in voxelized geometries [71].

To become a reliable tool, it is very important to ensure that the code has been properly validated for the simulation of the relevant types of interactions taking place within a microdosimeter. Indeed, measurements carried out with microdosimeters of different types have been used to assess the accuracy of these codes at microscale measurements, not only for track structure but also for fragmentation of ion beams, by means of experimental microdosimetry distributions [72] or radial dose profiles [73, 74].

It is worth to mention that all general-purpose codes cited above use a condensed history approach to model the electronic interactions of charged particles with matter. This approach allows an increase of computational efficiency by grouping a certain number of electronic collisions within a single simulation step; in addition, secondary electrons set in motion below a given threshold are not explicitly tracked, so that its energy is considered to have been deposited at the volume where the ionization occurred. For instance, the minimum threshold that can be set in FLUKA is 1 keV, whereas for some physics lists of the Geant4 toolkit, it can be as low as 100 eV. Thus, it is expected that the accuracy of calculations using the condensed history methods may not be optimal for submicrometric sensitive volumes, especially if electron transport plays a significant role. Actually, it has been found that FLUKA can reproduce satisfactorily lineal energy distributions obtained with a TEPC down to an equivalent size of 25 nm for carbon ion tracks, but not for proton tracks due to the typically longer range of secondary electrons in proton tracks at therapeutic energies [75, 76]. More accurate calculations can be achieved with track structure Monte Carlo codes, in which single electronic collisions are one by one simulated and all secondary electrons are produced (and thus less efficient in terms of computing time). Nevertheless, this improved spatial accuracy can be jeopardized by the uncertainties on individual interaction cross sections.

An example of pure track structure code for ion tracks in liquid water is PARTRAC [77]. In this sense, the Geant4 toolkit incorporates the extension Geant4-DNA, which includes interaction models and cross sections for electrons in liquid water down to 9 eV, protons and alphas down to 100 eV, and ions down to 0.5 MeV/u, as well as diffusion of radicals in liquid water [78–81]. Also, Geant4 incorporates a track structure extension for silicon material, Geant4-MicroElec, modeling electrons down to 16 eV and protons and ions down to 50 keV/u [82].

Monte Carlo codes can be used to generate libraries of microdosimetric quantities to be incorporated into treatment planning systems for radiobiology optimizations. In this sense, recent works [83, 84] suggest that modeling mean values and standard deviations of microdosimetric quantities is sufficient in

order to produce a comprehensive data set for proton therapy treatment planning systems.

Further, TOPAS framework [85], which wraps the Geant4 toolkit, has recently incorporated an extension providing users with the possibility of calculating microdosimetry spectra [86].

CONCLUSIONS

In ion therapy, beam quality assurance cannot be reduced to the correctness of the delivered absorbed dose alone. That is the case because the biological/clinical effect depends also on the **RBE** of the mixed radiation field, which in turn varies with depth. The lineal energy (y) spectrum measured with a microdosimeter is an adequate methodological approach to monitor the stochastic distributions of the energy deposited at the microscopic level, and the mean values of these distributions correlate strongly with the calculated $\overline{LET}_D$. Based on the measured y–distribution *via* application of a biological weighting function, or based on measured saturation-corrected dose mean lineal energy values y^* *via* the modified MKM, the **RBE$_{10}$** of proton and carbon ion therapeutic beams can be estimated. These estimations are in good agreement with radiobiological data. However, the optimal exploitation of microdosimeters in clinic is still under experimental investigation. Experimental microdosimetry offers valuable tools for the quality assurance of **LET**-based treatment plans, for the validation of Monte Carlo simulations, for the intercomparison of different therapeutic centers, and more in general to improve the understanding of underlying physical characteristics of the radiation interaction that correlate with different biological effectiveness.

AUTHOR CONTRIBUTIONS

PC drafted the manuscript, the Introduction, and the Conclusion. PC and VC contributed to the description of the microdosimetric detectors, their use in proton and carbon-ion beams to assess LET and RBE (sections from Assessing Variations of Linear Energy Transfer in Proton Data, The Microdosimeter as Relative Biological Effectiveness Monitor, The Microdosimeter to Monitor Relative Biological Effectiveness, Proton Data, How to Use Relative Biological Effectiveness Microdosimetric Assessment Values in a Therapeutic Plan: An Example, and Microdosimetric Monitoring of Therapeutic Carbon Ion Beams). HP and GM contributed to the prospective in carbon-ion therapy (section Prospective of Microdosimetry in the Clinics). MC-G contributed to the MC aspects (section Monte Carlo Codes in Microdosimetry). All authors contributed to improvements, corrections, and approval of the final version.

FUNDING

REFERENCES

1. Scholz M, Friedrich T, Magrin G, Colautti P, Petrovic I, Ristić-Fira A. Characterizing radiation effectiveness in ion beam therapy Part I: introduction and biophysical modelling of RBE, Using the LEMIV. *Front Phys.* (2020) **8**:272. doi: 10.3389/fphy.2020.00272

2. Relative Biological Effectiveness in Ion Beam Therapy. IAEA Technical Reports Series No. 461. English.

3. ICRU. *Fundamental Quantities and Units for Ionizing Radiation*, International Commission on Radiation Units and Measurements, ICRU Report 60. Bethesda, MD, (1998).

4. ICRU. *Microdosimetry, International Commission on Radiation Units and Measurements,* ICRU Report 36. Bethesda, MD, (1983).

5. Booz J. Mapping of fast neutron radiation quality. In: Burger G, Ebert HG, editors. *Proceedings of the Third Symposium on Neutron Dosimetry in Biology and Medicine*, Report No. EUR 5848, Luxembourg: Commission of the European Communities (1978).

6. Lindborg L, Waker A. *Microdosimetry: Experimental Methods and Applications.* Boca Raton, FL: CRC Press Taylor & Francis Group (2017) doi: 10.1201/9781315373737

7. Friedrich T, Scholz U, Elsässer T, Durante M, Scholz M. Systematic analysis of RBE and related quantities using a database of cell survival experiments with ion beam irradiation. *J Radiat Res.* (2013) **54-3**:494–514. doi: 10.1093/jrr/rrs114

8. Colautti P, Conte V, Selva A, Chiriotti S, Pola A, Bortot D, et al. Miniaturized microdosimeters as LET monitors: first comparison of calculated and experimental data performed at the 62 MeV/u ^{12}C beam of INFN-LNS with four different detectors. *Phys Med.* (2018) **52**:113–21. doi: 10.1016/j.ejmp.2018.07.004

9. Belli M, Cherubini R, Finotto S, Moschihi G, Sapora O, Tabocchini MA. RBE-LET relationship for the survival of V79 cells irradiated with low energy protons. *Int J Radiat Biol.* (1989) **55**:93–104. doi: 10.1080/09553008914550101

10. Bolst D, Guatelli S, Tran LT, Chartier L, Lerch MLF, Matsufuji N, et al. Correction factors to convert microdosimetry measurements in silicon to tissue in 12C ion therapy. *Phys Med Biol.* (2017) **62**:2055–69. doi: 10.1088/1361-6560/aa5de5

11. ICRU. Fundamental quantities and units for ionizing radiation, International Commission on Radiation Units and Measurements, ICRU report 85. *J ICRU.* (2011) **11**:1–31. doi: 10.1093/jicru_ndr011

12. Kellerer AM. Chord-length distributions and related quantities for spheroids. *Radial Res.* (1984) **98**:425–37. doi: 10.2307/3576477

13. Agosteo S, Colautti P, Fanton I, Fazzi A, Introini MV, Moro D, et al. Study of a solid state microdosemeter based on a monolithic silicon telescope: irradiations with low-energy neutrons and direct comparison with a cylindrical TEPC. *Radiat Prot Dosimetry.* (2011) **143**:432–5. doi: 10.1093/rpd/ncq481

14. De Nardo L, Cesari V, Donà G, Magrin G, Colautti P, Conte V, Tornielli G. Mini-TEPCs for radiation therapy. *Radiat Prot Dosimetry.* (2004) **108**:345–52 doi: 10.1093/rpd/nch023

15. Rosenfeld AB. Novel detectors for silicon based microdosimetry, their concepts and applications. NIM A. 809, 156–70, 2016. Advanced in Detectors and Application for Medicine. Fabio Sauli, Alberto Del Guerra, Alessandro Olivo and Peter Thirolf Editor. doi: 10.1016/j.nima.2015.08.059

16. Prieto-Pena J, Gómez F, Fleta C, Guardiola C, Pellegrini G, Donetti M, et al. Microdosimetric spectra measurements on a clinical carbon beam at nominal therapeutic fluence rate with silicon cylindrical microdosimeters. *IEEE Trans. Nuclear Sci.* (2019) **66–7**:1840–7. doi: 10.1109/TNS.2019.2921453

17. Tran LT, Chartier L, Prokopovich DA, Bolst D, Povoli M, ummanwar A, et al. Thin silicon microdosimeter utilizing 3D MEMS technology: charge collection study and its application in mixed radiation fields. *IEEE Trans Nuclear Sci.* (2018) **65**:467–472. doi: 10.1109/TNS.2017.2768062

18. Verona C, Magrin G, Solevi P, Bandorf M, Marinelli M, Stock M, et al. Toward the use of single crystal diamond based detector for ion-beam therapy microdosimetry. *Radiat Meas.* (2018) **110**:25–31. doi: 10.1016/j.radmeas.2018.02.001

19. Galer S, Hao L, Gallop J, Palmans H, Kirkby KJ, Nisbet A. Design concept for a novel SQUID-based microdosimeter. *Radiat Prot Dos.* (2011) **143**:427–31. doi: 10.1093/rpd/ncq475

20. Fathi K, Galer S, Kirkby KJ, Palmans H, Nisbet A. Coupling monte carlo simulations with thermal analysis for correcting microdosimetric spectra from a novel micro-calorimeter. *Rad Phys Chem.* (2017) **140**:406–11. doi: 10.1016/j.radphyschem.2017.02.055

21. Mazzucconi D, Bortot D, Agosteo S, Pola A, Pasquato S, Fazzi A, et al. Microdosimetry at nanometric scale with an avalanche-confinement tepc: response against a helium ion beam. *Rad Protect Dosimetry.* (2019) **183**:177–81. doi: 10.1093/rpd/ncy230

22. Bradley PD, Rosenfeld AB, Zaider M. Solid state microdosimetry. *Nuclear Instr Methods Phys Res Sec B.* (2001) **184**:135–57. doi: 10.1016/S0168-583X(01)00715-7

23. Tran LT, Chartier L, Bolst D, Pogossov A, Guatelli S, Petasecca M, et al. Characterization of proton pencil beam scanning and passive beam using a high spatial resolution solid-state microdosimeter. *Med Phys.* (2017) **44**:6085–95. doi: 10.1002/mp.12563

24. Farahmand M, Bos AJ, De Nardo L, van Eijk CW. First microdosimetric measurements with a TEPC based on a GEM. *Rad Protect Dosimetry.* (2004) **110**:839–43. doi: 10.1093/rpd/nch144

25. Shin J, Cho S, Park S, Lee S, Kwak J, Kim S, et al. SU-E-T-234: LET measurement using nuclear emulsion and monte carlo simulation for proton beam. *Med Phys.* (2012) **39**:3757. doi: 10.1118/1.4735297

26. Paganetti H. Relative biological effectiveness (RBE) values for proton beam therapy. Variations as a function of biological endpoint, dose, and linear energy transfer. *Phys Med Biol.* (2014) **59**:R419–72. doi: 10.1088/0031-9155/59/22/R419

27. Wagenaar D, Tran LT, Meijers A, Marmitt GG, Souris K, Bolst D, et al. Validation of linear energy transfer computed in a monte carlo dose engine of a commercial treatment planning system. *Phys Med Biol.* (2020) **65**:025006. doi: 10.1088/1361-6560/ab5e97

28. ICRU. *Linear Energy Transfer, International Commission on Radiation Units and Measurements*, ICRU Report 16, Washington, DC, (1970).

29. Conte V, Bianchi A, Selva A, Petringa G, Cirrone GAP, Parisi A, et al. Microdosimetry at CATANA 62 MeV proton beam with a sealed miniaturized TEPC. *Phys Med.* (2019) **64**:114–22. doi: 10.1016/j.ejmp.2019.06.011

30. De Nardo L, Colautti P, Hérault J, Conte V, Moro D. Microdosimetric characterisation of a therapeutic proton beam used for conjunctival melanoma treatments. *Radiat Meas.* (2010) **45**:1387–90. doi: 10.1016/j.radmeas.2010.05.034

31. Magrin G, Verona C, Ciocca M, Marinelli M, Mastella E, Stock M, et al. Microdosimetric characterization of clinical carbon-ion beams using synthetic diamond detectors and spectral conversion methods. *Med Phys.* (2020) **47**:713–21. doi: 10.1002/mp.13926

32. Petringa G, Pandola L, Agosteo S, Catalano R, Colautti P, Conte V, et al. Monte Carlo implementation of new algorithms for the averaged-dose and -track linear energy transfer evaluation in 62 MeV clinical proton beams. *Phys Med Biol.* (2020). doi: 10.1088/1361-6560/abaeb9

33. Palmans H, Rabus H, Belchior AL, Bug MU, Galer S, Giesen U, et al. Future development of biologically relevant dosimetry. *Br J Radiol.* (2015) **87**:20140392. doi: 10.1259/bjr.20140392

34. Pihet P, Menzel HG, Schmidt R, Beauduin M, Wambersie A. Biological weighting function for rbe specification of neutron therapy beams. Intercomparison of 9 European centres. *Radiat Prot Dosim.* (1990) **31**:1-4. doi: 10.1093/oxfordjournals.rpd.a080709

35. Loncol T, Cosgrove V, Denis JM, Gueulette J, Mazal A, Menzel HG, et al. Radiobiological effectiveness of radiation beams with broad LET spectra: microdosimetric analysis using biological weighting functions. *Radiat Prot Dosim.* (1994) **52**:347–52. doi: 10.1093/rpd/52.1-4.347

36. Tung CJ. Microdosimetric relative biological effectiveness of therapeutic proton beams. *Biomed J.* (2015) **38**:399–407. doi: 10.4103/2319-4170.167072

37. Gueulette J, Bohm L, Slabbert JP, De Coster BM, Rutherfoord GS, Ruifrok A, et al. Proton relative biological effectiveness (RBE) for survival in mice after

38. Gueulette J, Slabbert JP, Böhm L, De Coster BM, Rosier JF, Octave-Prignot M, et al. Proton RBE for early intestinal tolerance in mice after fractionated irradiation. *Radiother Oncol.* (2001) **61**:177–84. doi: 10.1016/S0167-8140(01)00446-7

39. Gueulette J, Blattmann H, Pedroni E, Coray A, De Coster BM, Mahy P, et al. Relative biologic effectiveness determination in mouse intestine for scanning proton beam at Paul Scherrer Institute, Switzerland. Influence of motion. *Int J Radiat Oncol Biol Phys.* (2005) **62**:838–45. doi: 10.1016/j.ijrobp.2005.03.048

40. Gueulette J, Boehm L, De Coster B-M, Vynckier S, Octave-Prignot M, Schreuder AN, et al. RBE variation as a function of depth in the 200 MeV proton beam produced at the national accelerator centre in faure (South Africa). *Radiother Oncol.* (1997) **42**:303–9 doi: 10.1016/S0167-8140(97)01919-1

41. Gueulette J, Gregoire V, Octave-Prignot M, Wambersie A. Measurements of radiobiological effectiveness in the 85 MeV proton beam produced at the cyclotron CYCLONE of Louvain-la-Neuve. *Belgium Radiat Res.* (1996) **145**:70–4. doi: 10.2307/3579197

42. Uzawa A, Ando K, Furusawa Y, Kagiya G, Fuji H, Hata M, et al. Biological intercomparison using gut crypt survivals for proton and Carbon-ion beams. *J Radiat Res.* (2007) **48**:A75–80. doi: 10.1269/jrr.48.A75

43. Mason KA, Gillin MT, Mohan R, Cox JD. Preclinical biologic assessment of proton beam relative biologic effectiveness at proton therapy center Houston. *Int J Radiat Oncol Biol Phys.* (2007) **68**:968–70. doi: 10.1016/j.ijrobp.2007.03.051

44. De Nardo L, Cesari V, Iborra N, Conte V, Colautti P, Herault J, et al. Microdosimetric assessment of nice therapeutic proton beam biological quality. *Phys Med.* (2004) **20**:71–77. doi: 10.1093/rpd/ncq483

45. De Nardo L, Dal Corso F, Pegoraro M. Microdosimetric measurements in gamma and neutron fields with a tissue-equivalent proportional counter based on a gas electron multiplier. *Rad Prot Dosim.* (2017) **175**:260–66. doi: 10.1093/rpd/ncw294

46. Gerlach R, Roos H, Kellerer AM. Heavy Ion RBE and microdosimetric spectra. *Radiat Prot Dosim.* (2002) **99**:413–8. doi: 10.1093/oxfordjournals.rpd.a006821

47. Kase Y, Kanai T, Sakama M, Tameshige Y, Himukai T, Nose H, et al. Microdosimetric approach to NIRS-defined biological dose measurement for carbon-ion treatment beam. *J Radiat Res.* (2011) **52**:59–68. doi: 10.1269/jrr.10062

48. Tran LT, Chartier L, Prokopovich DA, Reinhard MI, Petasecca M, Guatelli S, et al. 3D-mesa "bridge" silicon microdosimeter: charge collection study and application to RBE studies in 12C radiation therapy. *IEEE Trans Nuclear Sci.* (2015) **148**:44–51. doi: 10.1109/TNS.2015.2391102

49. PTCOG, *Particle Therapy Co-Operative Group Website.* Available online at: https://www.ptcog.ch/index.php/facilities-in-operation (accessed April 6, 2020).

50. Bassler N, Jäkel O, Søndergaard CS, Petersen JB. Dose- and LET-painting with particle therapy. *Acta Oncol.* (2010) **49**:1170–6. doi: 10.3109/0284186X.2010.510640

51. Bassler N, Toftegaard J, Lühr A, Sørensen BS, Scifoni E, Krämer M, et al. LET-painting increases tumour control probability in hypoxic tumours. *Acta Oncol.* (2014) **53**:25–32. doi: 10.3109/0284186X.2013.832835

52. Tinganelli W, Durante M, Hirayama R, Krämer M, Maier A, Kraft-Weyrather W, et al. Kill-painting of hypoxic tumours in charged particle therapy. *Sci Rep.* (2015) **5**:17016. doi: 10.1038/srep17016

53. Martino G, Durante M, Schardt D. Microdosimetry measurements characterizing the radiation fields of 300 MeV/u 12C and 185 MeV/u 7Li pencil beams stopping in water. *Phys Med Biol.* (2010) **55**:3441–9. doi: 10.1088/0031-9155/55/12/011

54. Alrowaili ZA, Lerch MLF, Petasecca M, Carolan MG, Metcalfe PE, Rosenfeld AB. Beam perturbation characteristics of a 2D transmission silicon diode array, magic plate. *J Appl Clin Med Phys.* (2016) **17**:85–98. doi: 10.1120/jacmp.v17i2.5932

55. Conte V, Colautti P, Chiriotti S, Moro D, Ciocca M, Mairani A. Mini-TEPC microdosimetric study of carbon ion therapeutic beams at CNAO. *EPJ Web Conf.* (2017) **153**:01012. doi: 10.1051/epjconf/201715301012

56. Magrin G. A method to convert spectra from slab microdosimeters in therapeutic ion-beams to the spectra referring to microdosimeters

of different shapes and material. *Phys Med Biol.* (2018) **63**:215021. doi: 10.1088/1361-6560/aae655

57. Hagiwara Y, Bhattacharyya T, Matsufuji N, Isozaki Y, Takiyama H, Nemoto K, et al. Influence of dose-averaged linear energy transfer on tumour control after carbon-ion radiation therapy for pancreatic cancer. *Clin Transl Radiat Oncol.* (2020) **21**:19–24. doi: 10.1016/j.ctro.2019.11.002

58. Battistoni G, Bauer J, Boehlen TT, Cerutti F, Chin MPW, Dos Santos Augusto R, et al. The fluka code: an accurate simulation tool for particle therapy. *Front Oncol.* (2016) **6**:116. doi: 10.3389/fonc.2016.00116

59. Agostinelli S, Allison J, Amako K, Apostolakis J, Araujo H, Arce P, et al. Geant4—a simulation toolkit. *Nucl Instruments Methods Phys Res Sect A.* (2003) **506**:250–303. doi: 10.1016/S0168-9002(03)01368-8

60. Allison J, Amako K, Apostolakis J, Araujo H, Arce Dubois P, Asai M, et al. Geant4 developments and applications. *IEEE Trans Nucl Sci.* (2006) **53**:270–8. doi: 10.1109/TNS.2006.869826

61. Allison J, Amako K, Apostolakis J, Arce P, Asai M, Aso T, et al. Recent developments in Geant4. *Nucl Instr Methods Phys Res Sect A.* (2016) **835**:186–225. doi: 10.1016/j.nima.2016.06.125

62. Sato T, Iwamoto Y, Hashimoto S, Ogawa T, Furuta T, Abe S, et al. Features of Particle and Heavy Ion Transport code System (PHITS) version 3.02. *J Nucl Sci Technol.* (2018) **55**:684–90. doi: 10.1080/00223131.2017.1419890

63. Guardiola C, Quirion D, Pellegrini G, Fleta C, Esteban S, Cortés-Giraldo MA, et al. Silicon-based three-dimensional microstructures for radiation dosimetry in hadrontherapy. *Appl Phys Lett.* (2015) **107**:023505. doi: 10.1063/1.4926962

64. Galer S, Shipley DR, Palmans H, Kirkby KJ, Nisbet A. Monte Carlo simulation of a TEPC for microdosimetry of carbon ions. *Rad Phys Chem.* (2017) **140**:412–8. doi: 10.1016/j.radphyschem.2017.02.028

65. Livingstone J, Prokopovich DA, Tran LT, Guatelli S, Petasecca M, Lerch MLF, et al. Charge collection in n-SOI planar microsimeters. *IEEE Trans Nucl Sci.* (2013) **60**:4289–96. doi: 10.1109/TNS.2013.2283307

66. Gómez F, Fleta C, Esteban S, Quirion D, Pellegrini G, Lozano M, et al. Measurement of carbon ion microdosimetric distributions with ultrathin 3D silicon diodes. *Phys Med Biol.* (2016) **61**:4036–47. doi: 10.1088/0031-9155/61/11/4036

67. Bianchi A, Selva A, Colautti P, Bortot D, Mazzucconi D, Pola A, et al. Microdosimetry with a sealed mini-TEPC and a silicon telescope at a clinical proton SOBP of CATANA. *Radiat Phys Chem.* (2020) **171**:108730. doi: 10.1016/j.radphyschem.2020.108730

68. Burigo L, Pshenichnov I, Mishustin I, Bleicher M. Microdosimetry spectra and RBE of 1H, 4He, 7Li and 12C nuclei in water studied with Geant4. *Nucl Instr Methods Phys Res Sect B.* (2014) **320**:89–99. doi: 10.1016/j.nimb.2013.10.018

69. Agosteo S, Introini MV, Pola A, Sagia E. Response of a silicon telescope microdosimeter to 400 AMeV carbon ions. *Radiat Meas.* (2014) **71**:524–8. doi: 10.1016/j.radmeas.2014.05.023

70. Anjomani Z, Hanu AR, Prestwich WV, Byun SH. Monte Carlo design study for thick gas electron multiplier-based multi-element microdosimetric detector. *Nucl Instr Methods Phys Res Sect A.* (2014) **757**:67–74. doi: 10.1016/j.nima.2014.04.063

71. Cortés-Giraldo MA, Carabe A. A critical study of different Monte Carlo scoring methods of dose average linear-energy-transfer maps calculated in voxelized geometries irradiated with clinical proton beams. *Phys Med Biol.* (2015) **60**:2645–69. doi: 10.1088/0031-9155/60/7/2645

72. Bolst D, Guatelli S, Tran LT, Chartier L, Davis J, Biasi G, et al. Validation of Geant4 for silicon microdosimetry in heavy ion therapy. *Phys Med Biol.* (2020) **65**:045014. doi: 10.1088/1361-6560/ab586a

73. Incerti S, Psaltaki M, Gillet P, Barberet P, Bardiès M, Bernal MA, et al. Simulating radial dose of ion tracks in liquid water simulated with Geant4-DNA: a comparative study. *Nucl Instruments Methods Phys Res Sect B.* (2014) **333**:92–8. doi: 10.1016/j.nimb.2014.04.025

74. Tsuda S, Sato T, Ogawa T. Measurement of the stochastic radial dose distribution for a 30-MeV proton beam using a wall-less tissue-equivalent proportional counter. *Radiat Prot Dosimetry.* (2015) **168**:190–6. doi: 10.1093/rpd/ncv285

75. Mazzucconi D, Bortot D, Pola A, Agosteo S, Pasquato S, Fazzi A, et al. Monte Carlo simulation of a new TEPC for microdosimetry at nanometric level: response against a carbon ion beam. *Radiat Meas.* (2018) **113**:7–13. doi: 10.1016/j.radmeas.2018.03.006

76. Mazzucconi D, Bortot D, Pola A, Fazzi A, Colautti P, Conte V, et al. Nano-microdosimetric investigation at the therapeutic proton irradiation line of CATANA. *Radiat Meas.* (2019) **123**:26–33. doi: 10.1016/j.radmeas.2019.02.012

77. Friedland W, Kundrát P, Becker J, Eidemüller M. Biophysical simulation tool partrac: modelling proton beams at therapy-relevant energies. *Radiat Prot Dosimetry.* (2019) **186**:172–5. doi: 10.1093/rpd/ncz197

78. Incerti S, Kyriakou I, Bernal MA, Bordage MC, Francis Z, Guatelli S, et al. Geant4-DNA example applications for track structure simulations in liquid water: a report from the Geant4-DNA Project. *Med Phys.* (2018) **45**:e722–39. doi: 10.1002/mp.13048

79. Bernal MA, Bordage MC, Brown JMC, Davídková M, Delage E, El-Bitar Z, et al. Track structure modeling in liquid water: a review of the Geant4-DNA very low energy extension of the Geant4 Monte Carlo simulation toolkit. *Phys Med.* (2015) **31**:861–74. doi: 10.1016/j.ejmp.2015.10.087

80. Incerti S, Ivanchenko A, Karamitros M, Mantero A, Moretto P, Tran HN, et al. Comparison of GEANT4 very low energy cross section models with experimental data in water. *Med Phys.* (2010) **37**:4692–708. doi: 10.1118/1.3476457

81. Li J, Li C, Qiu R, Yan C, Xie W, Wu Z, et al. DNA strand breaks induced by electrons simulated with Nanodosimetry Monte Carlo Simulation Code: NASIC. *Radiat Prot Dosimetry.* (2015) **166**:38–43. doi: 10.1093/rpd/ncv171

82. Raine M, Gaillardin M, Paillet P. Geant4 physics processes for silicon microdosimetry simulation: improvements and extension of the energy-range validity up to 10 GeV/nucleon. *Nucl Instruments Methods Phys Res Sect B Beam Interact with Mater Atoms.* (2014) **325**:97–100. doi: 10.1016/j.nimb.2014.01.014

83. Bertolet A, Baratto-Roldán A, Cortés-Giraldo MA, Carabe-Fernandez A. Segment-averaged LET concept and analytical calculation from microdosimetric quantities in proton radiation therapy. *Med Phys.* (2019) **46**:4204–14. doi: 10.1002/mp.13673

84. Bertolet A, Cortés-Giraldo MA, Carabe-Fernandez A. On the concepts of dose-mean lineal energy, unrestricted and restricted dose-averaged LET in proton therapy. *Phys Med Biol.* (2020) **65**:075011. doi: 10.1088/1361-6560/ab730a

85. Perl J, Shin J, Schümann J, Faddegon B, Paganetti H. TOPAS: an innovative proton Monte Carlo platform for research and clinical applications. *Med Phys.* (2012) **39**:6818–37. doi: 10.1118/1.4758060

86. Zhu H, Chen Y, Sung W, McNamara AL, Tran LT, Burigo LN, et al. The microdosimetric extension in TOPAS: development and comparison with published data. *Phys Med Biol.* (2019) **64**:145004. doi: 10.1088/1361-6560/ab23a3